Phase transformations in microcrystalline cellulose due to partial dissolution

Benoît J.-C. Z. Duchemin · Roger H. Newman · Mark P. Staiger

Abstract All-cellulose composites were prepared by partly dissolving microcrystalline cellulose (MCC) in an 8.0 wt% LiCl/DMAc solution, then regenerating the dissolved portion. Wide-angle X-ray scattering (WAXS) and solid-state ^{13}C NMR spectra were used to characterize molecular packing. The MCC was transformed to relatively slender crystallites of cellulose I in a matrix of paracrystalline and amorphous cellulose. Paracrystalline cellulose was distinguished from amorphous cellulose by a displaced and relatively narrow WAXS peak, by a 4 ppm displacement of the C-4 ^{13}C NMR peak, and by values of $T_2(H)$ closer to those for crystalline cellulose than disordered polysaccharides. Cellulose II was not formed in any of the composites studied. The ratio of cellulose to solvent was varied, with greatest consequent transformation observed for $c < 15\%$, where c is the weight of cellulose expressed as % of the total weight of cellulose, LiCl and DMAc. The dissolution time was varied between 1 h and 48 h, with only small additional changes achieved by extension beyond 4 h.

Abbreviations

MCC	Microcrystalline cellulose
DMAc	*N,N*-dimethylacetamide
NMR	nuclear magnetic resonance
WAXS	Wide-angle X-ray scattering

B. J.-C.Z. Duchemin (✉) · M. P. Staiger
Department of Mechanical Engineering, University of Canterbury, Private Bag 4800, Christchurch, New Zealand
e-mail: bjd51@student.canterbury.ac.nz

R. H. Newman
Scion, Private Bag 3020, Rotorua, New Zealand

Introduction

Crystalline cellulose I has a tensile modulus of 138 GPa (Nishino et al. 1995) and an ultimate tensile strength of at least 2 GPa (Kroon-Batenburg et al. 1990; Yano et al. 2005), based on experimental data. If values as high as these could be achieved in reinforcement for composite materials, cellulose I could compete with steel or high-performance synthetic fibres (Nishino et al. 2004; Yano et al. 2005). Failure to achieve such high performance has been attributed to poor bonding between polar cellulosic fibres and less-polar polymer matrices (Bledzki and Gassan 1999; Lu and Wu 2000). Fibre-matrix compatibility can be improved by using cellulose itself as the matrix. Nishino et al. (2004) were the first to take this approach, introducing a new class of high

strength, biodegradable materials known as all-cellu-
lose composites.

While the mechanical properties of all-cellulose
composites are known, there are very few references
to the nature of the molecular packing in the matrix
(Gindl and Keckes 2005). We sought insights from
studies based on X-ray diffraction and solid-state ^{13}C
NMR spectroscopy.

Two distinct strategies have been used in prepa-
ration of all-cellulose composites.

(1) *Regeneration*. Nishino et al. (2004) dissolved
    kraft fibre and regenerated the cellulose in the
    presence of ramie fibres.
(2) *Partial dissolution*. Gindl and Keckes (2005)
    and Gindl et al. (2006a, b) partly dissolved
    cellulose I and precipitated the dissolved portion
    to form a matrix around the undissolved portion.

Similar composites have also been prepared by using
esters such as cellulose acetate butyrate (CAB) as the
matrix (Glasser et al. 1999; Gindl and Keckes 2004).
While those composites were based primarily on
cellulose, esterification altered the polarity of the
matrix relative to the fibres and mechanical perfor-
mance was not as good as for true all-cellulose
composites. Gindl and Keckes (2004) reported a
tensile strength of 129 MPa for CAB reinforced with
bacterial cellulose, compared with 480 MPa for a true
all-cellulose composite prepared by regeneration
(Nishino et al. 2004).

We chose to follow Nishino et al. (2004), Gindl
and Keckes (2005) and Gindl et al. (2006a, b) in
preparing all-cellulose composites by partial dissolu-
tion in lithium chloride/N,N-dimethylacetamide
(LiCl/DMAc).

Experimental

Preparation of composites

Cellulose dissolution using DMAc initially involves
an activation step in which the cellulose structure is
first swollen via solvent exchange (Striegel 2002;
Dupont 2003). The increased molecular mobility of
cellulose allows the LiCl/DMAc solvent to penetrate
the cellulose structure more easily (McCormick et al.
1985; Ishii et al. 2003). In the present work,
microcrystalline cellulose (MCC) powder (Avicel,

Merck, particle size between 20 μm and 160 μm)
was immersed in distilled water at 20 °C for 48 h and
vacuum-filtered through Whatman No. 1 filter paper,
twice immersed in acetone (Biolab, laboratory grade)
at 20 °C for 24 h and filtered through Whatman
No. 1 filter paper to remove the acetone each time,
twice immersed in DMAc (Merck, synthesis grade)
at 20 °C for 24 h and each time filtered through
Whatman No. 1 filter paper afterward, vacuum-dried
for 48 h at 60 °C and then sieved (90 μm). The
activated MCC was vacuum-dried for a further
48 hrs at 60 °C and finally sealed in a container
for storage.

Partial dissolution

A solution of 8.0% (by total weight) LiCl in DMAc
was prepared by mixing LiCl (Unilab, 99% purity)
and DMAc in a 2 L Schott bottle. The bottle was
immediately sealed to prevent moisture absorption.
The mixture was mechanically stirred for 24 h until
the salt appeared to be completely dissolved.

A portion of 1 g activated MCC was immersed in
a Petri dish containing sufficient LiCl/DMAc to
achieve cellulose concentrations of c = 5%, 10%,
15% or 20%, where c is expressed as % of the total
weight of cellulose, LiCl and DMAc. The solution
was placed under vacuum and stirred for 1 h, 4 h,
8 h or 48 h at 20 °C. The regeneration of the
dissolved cellulose began initially with light spray-
ing of water onto the surface of the gel in order to
fix the shape of the final sample. The partially
regenerated gel was then carefully transferred to a
beaker and immersed in water for 48 h at 20 °C. The
water was changed at least every 24 h. Residual LiCl
or DMAc was removed by further thorough rinsing
of the specimen with water. The specimens were
then dried 48 h in a vacuum oven at 60 °C to ensure
complete solidification.

Wide Angle X-ray Scattering (WAXS)

WAXS was performed on as-received MCC, acti-
vated MCC and on the final composites. X-ray
patterns were obtained with a Philips PW1729
diffractometer using Cu K$_\alpha$ radiation
(λ = 0.15418 nm), voltage of 50 kV and current of
40 mA with 2θ increased in steps of 0.02°. The X-ray
data was smoothened over 30 adjacent points using

the adjacent averaging smoothing function in Origin© Pro 7.5 and plots were then area-normalized. Peaks were assigned according to the monoclinic unit cell described by Sugiyama et al. (1991). Peak positions and widths were measured from plots by using the method described by Gjønnes and Norman (1958). We did not use curve-fitting software because of the complexity of the diffractograms, with peak positions and widths expected to be related to crystallite dimensions as well as crystalline forms of cellulose, as discussed below. Instead, we confined precise measurements to samples that had not been in contact with LiCl/DMAc.

The Scherrer equation was used to calculate the crystal thickness by using the half-width at half-height of the peak assigned to (200) planes:

$$D = K\lambda/(B\cos\theta) \qquad (1)$$

where D is the crystal thickness, λ the radiation wavelength, θ the diffraction angle and B the full width of the diffraction peak measured at half maximum height prior to smoothing. The correction factor, K, was set to 0.9 (Murdock 1930). A crystallinity index CrI was used as defined by Segal et al. (1959):

$$\mathrm{CrI} = 100(I - I')/I \qquad (2)$$

Here I is the height of the peak assigned to (200) planes, typically located in the range $2\theta = 21°$ to $22°$, and I' is the height measured at $2\theta = 18°$, which is where the maximum appears in a diffractogram of amorphous cellulose.

Solid state ^{13}C nuclear magnetic resonance (NMR)

Each composite was crushed to particle dimensions of ~ 0.5 mm, combined with a similar or larger weight of water, and packed into a zirconium oxide rotor. Excess water was expelled during packing to prepare samples with a typical solids content of 55% by dry weight. The rotor was sealed with a Kel-F® cap.

Solid state CP-MAS ^{13}C NMR spectra were obtained on a Bruker Avance DRX200 FT-NMR spectrometer at a frequency of 50.3 MHz and at a magic-angle spinning frequency of 5 kHz. Each 90°

proton preparation pulse of 5 µs was followed by a delay τ, a contact time of 1 ms, acquisition time of 20 ms, and a recycle delay of 1 s. Two spectra were acquired for each sample and labeled **S** ($\tau = 1$ µs) and **S'** ($\tau = 15$ µs). Bold type is used for these symbols since they represent vectors, i.e., lists of the signal heights measured across a range of chemical shifts. Transients from a minimum of 10,000 pulses were averaged in both cases.

Signals from crystalline cellulose were partly suppressed in **S'**, through relatively rapid $T_2(H)$ decay during the delay τ. The discrimination was enhanced by proton spin relaxation editing (PSRE). This method is more commonly used to process spectra modified by rotating-frame relaxation (Newman 1999) but has been used to process spectra modified by $T_2(H)$ (Newman et al. 1996). PSRE involves computing linear combinations:

$$A = kS + k'S' \qquad (3a)$$

$$B = (1 - k)S - k'S' \qquad (3b)$$

The values of k and k' are adjusted until signals assigned to poorly ordered matter are excluded from **A** and signals assigned to well-ordered matter are excluded from **B**. In this case, signals at 80 ppm and 89 ppm were assigned to C-4 in poorly ordered and crystallite-interior cellulose, respectively (Newman 1999). Details concerning the adjustment of k and k' can be found elsewhere (Newman and Hemmingson 1995). The fraction F of crystalline cellulose in each composite was estimated by dividing the area of **A** by area of **S**.

The subspectra labeled **A** showed two partly resolved C-4 signals, assigned to crystallite-interior and crystallite-surface glucosyl residues, at 89 ppm and 84 ppm respectively. Signal areas were delimited by the baseline and a vertical line drawn at 86.4 ppm. Relative areas were used to estimate the percentage X of cellulose chains contained in crystallite interiors (Newman 1999). Assuming a simplified model of a square cellulose crystallite with cross-sectional dimensions $L \times L$ and only a monolayer of cellulose chains exposed to the surface, an estimate of the apparent average crystallite size can be given by the expression (Newman 1999):

$$L = 1.14/\left(1 - X^{1/2}\right) \qquad (4)$$

Results and discussion

WAXS diffractograms

Activation showed only a minor effect on the WAXS diffractogram (Fig. 1). The peak assigned to (200) planes appeared at $2\theta = 22.6°$ and $22.8°$ in as-received MCC and activated MCC, respectively, as in published WAXS diffractograms for cellulose I (Isogai et al. 1989; Ishii et al. 2003). The full widths B at half maximum height were $1.75°$ and $1.68°$, giving crystal thicknesses of 4.5 nm and 4.9 nm, respectively, according to Eq. (1).

Peaks at $2\theta = 15.1°$, $16.8°$ and $34.8°$ in the diffractogram for activated cellulose were also consistent with peaks in published WAXS diffractograms for cellulose I (Isogai et al. 1989; Ishii et al. 2003). The crystallinity index CrI calculated from Eq. (2) decreased from 87% for MCC to 80% after activation (Table 1).

The WAXS diffractograms for all-cellulose composites showed a small shoulder at $2\theta = 20.8°$ that progressively developed into a distinct diffraction peak with decreasing cellulose concentration in the solvent (Figs. 2, 3). The peak was more distinct in composites prepared with a dissolution time of 8 h
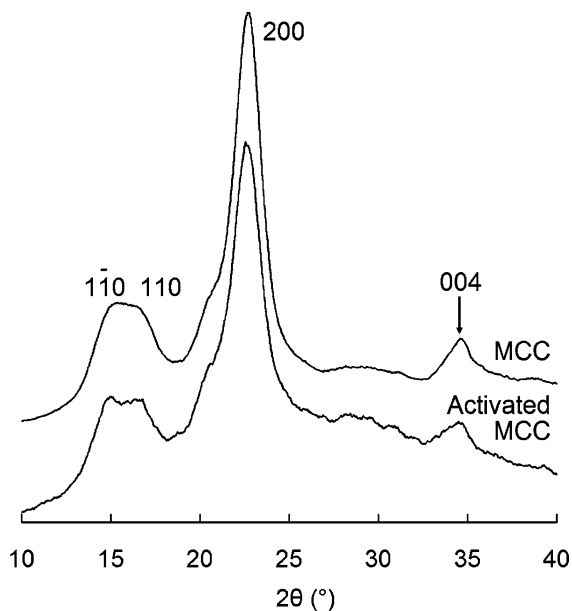
Fig. 1 WAXS diffractograms of MCC before and after activation. Peaks assignments use the monoclinic cellulose I unit cell of Sugiyama et al. (1991)

(Fig. 3), relative to 1 h (Fig. 2). Plots for other dissolution times indicated that equilibrium was reached after approximately 4 h, with little further change to 48 h. Gindl and Keckes (2005) observed this peak in WAXS diffractograms of all-cellulose composites, and assigned it to regenerated cellulose. They observed a similar peak in a WAXS diffractogram of cellulose produced by dissolving cellulose II in LiCl/DMAc and regenerating it.

The peak at $2\theta = 20.8°$ was $5.0°$ wide at half maximum height, and this width was too small for the peak to be assigned to amorphous cellulose. Ball-milled cellulose is commonly used as a reference standard for amorphous cellulose. The peak position has been reported as $2\theta = 18°$ (Segal et al. 1959; Mann 1962) or $2\theta = 20°$ (Schroeder et al. 1986), but it is generally agreed that the width is approximately $10°$. The width of $5.0°$, observed in Fig. 3, corresponds to a crystallite thickness of $D = 1.6$ nm according to Eq. (1). For (200) planes separated by 0.4 nm (Sugiyama et al. 1991) that corresponds to crystallites containing just 4 planes.

A commonly used crystallinity index CrI, expressed in Eq. (2), exploits the fact that the maximum for amorphous cellulose falls between peaks in the diffractogram for cellulose I. The diffractograms in Figs. 2 and 3 showed increasing height at $2\theta = 18°$, for increasing degrees of transformation, but the value of CrI never dropped below 39% (Table 1).

Gjønnes and Norman (1958) and Ioelovich and Larina (1999) reported lattice expansion in thin crystallites of cellulose I, so that an increase in peak width was associated with a displacement to low values of 2θ. A curve published by Gjønnes and Norman (1958) indicated that an increase in peak width to $7°$ was sufficient to displace the peak to $2\theta = 21°$. The peak at $2\theta = 20.8°$ in Figs. 2 and 3 is therefore consistent with cellulose I crystallites split to fine dimensions.

When regenerated cellulose crystallizes to the cellulose II allomorph it shows WAXS peaks at $2\theta = 12.1°$, $19.8°$ and $22.0°$ (Isogai et al. 1989). Changes in lattice dimensions influence the positions of WAXS peaks for cellulose II, but the pattern of displacements is different from that for cellulose I. Gjønnes and Norman (1960) showed that the peak at $2\theta = 19.8°$ is displaced to higher values, and the peak at $2\theta = 22.0°$ to lower values, as the peaks broaden. Extrapolation from their data suggested that the two
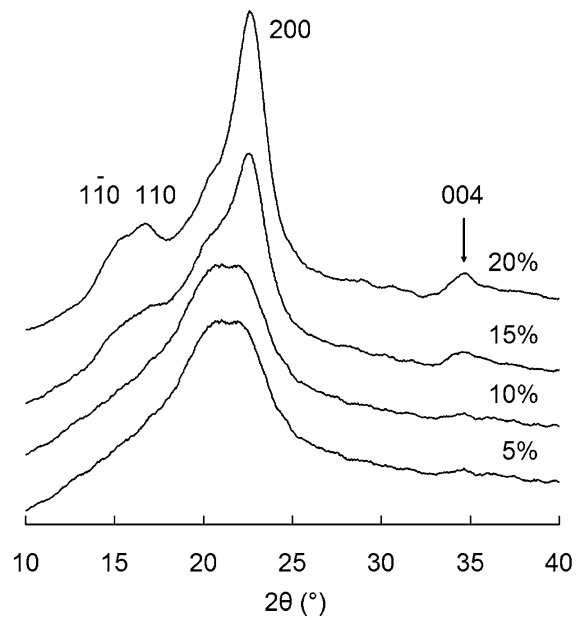
Table 1 Data for starting materials and all-cellulose composites prepared by partial dissolution for 8 h at cellulose concentrations c expressed as % of the total weight of cellulose, LiCl and DMAc

Sample	CrI (%)	D (nm)	F	X (%)	L (nm)
MCC	87	4.5	(0.84)[a]	(65)[a]	(5.9)[a]
Activated	80	4.8	0.73	67	6.3
$c = 20\%$	71	–[b]	0.56	61	5.2
$c = 15\%$	59	–[b]	0.52	49	3.8
$c = 10\%$	39	–[b]	0.24	32	2.6
$c = 5\%$	39	–[b]	0.37	24	2.3

[a] literature values (Newman and Hemmingson 1995)

[b] not done because of peak overlap
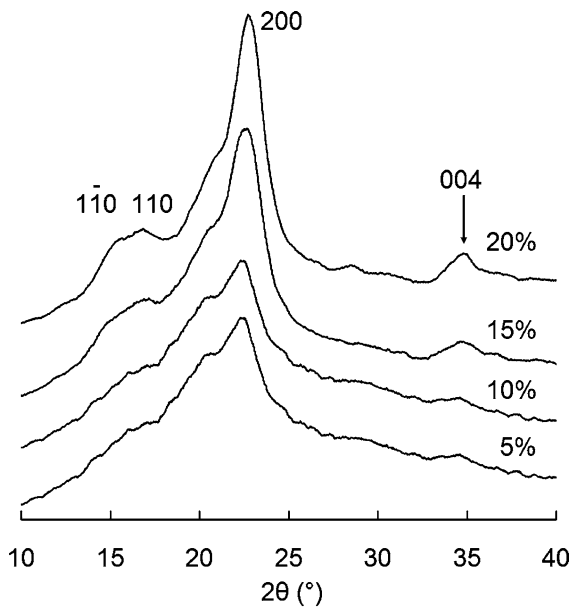
Fig. 2 WAXS diffractograms of all-cellulose composites prepared from activated cellulose by partial dissolution for 1 h with values of c shown above each trace

Fig. 3 WAXS diffractograms of all-cellulose composites prepared from activated cellulose by partial dissolution for 8 h with values of c shown above each trace

peaks might form a single peak, with a width of approximately $7°$, at a value of 2θ somewhere between $20°$ and $21°$. Yamashiki et al. (1992) confirmed movement towards an intermediate value of 2θ by published WAXS diffractograms for cellulose II as viscose and cuprammonium rayons, showing a broad peak at $2\theta = 20.0°$ with a shoulder at $2\theta = 21.6°$. The peak at $2\theta = 20.8°$ in Fig. 3 is therefore indistinguishable from the pattern predicted for very narrow crystallites of cellulose II.

Cellulose III, when prepared from cellulose I, shows a strong WAXS peak $2\theta = 20.7°$ and a weaker peak $2\theta = 11.7°$ (Isogai et al. 1989). The former peak
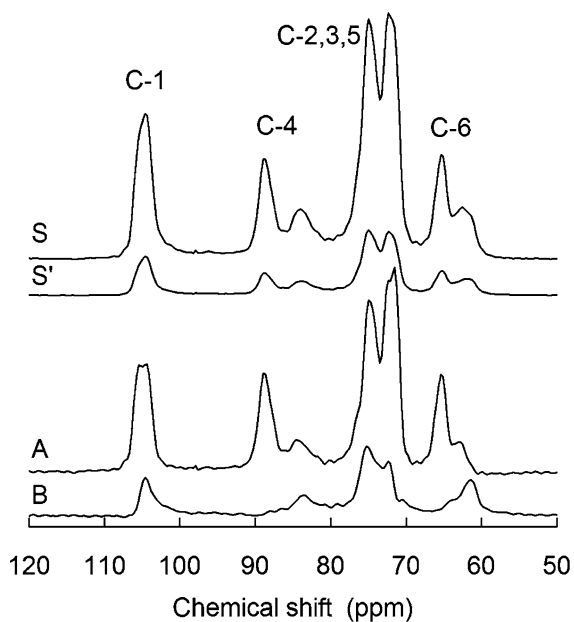
matched the broad peak in WAXS diffractograms of the most severely treated specimens (Figs. 2 and 3), but the latter was not observed.

The peak assigned to (200) planes of cellulose I remained visible as a shoulder at $2\theta = 22.3°$ in WAXS diffractograms of specimens with the greatest degrees of transformation, i.e., the lower two traces in Figs. 2 and 3. The shoulder was too weak for measurement of the peak width, but the curve published by Gjønnes and Norman (1958) indicated that displacement to $2\theta = 22.3°$ corresponded to a peak width of $3°$, for which Eq. (1) indicated a

crystallite thickness of approximately 3 nm. The diffractogram of MCC (Fig. 1) showed a peak assigned to (004) planes. This peak was weak or absent in diffractograms of all-cellulose composites prepared with the greatest degrees of transformation, e.g., the lowest diffractogram in Fig. 3. The disappearance of this peak suggests longitudinal disorder, consistent with a paracrystalline matrix.

Solid-state ^{13}C NMR

The ^{13}C NMR spectrum of activated MCC (Fig. 4) resembled a published spectrum of Avicel MCC (Newman and Hemmingson 1995), confirming WAXS indications of little change in molecular packing associated with activation. Minor changes were revealed by PSRE (Fig. 4). In the published PSRE results (Newman and Hemmingson 1995) subspectrum **A** accounted for 84% of the area of the total spectrum **S**. This proportion decreased to 73% after activation (Fig. 4), indicating transformation of some of the cellulose I to a less ordered form of cellulose. A published ^{13}C NMR study of Avicel MCC indicated a crystallite width of $L = 5.9$ nm (Newman 1999). Peak areas in subspectrum **A** of
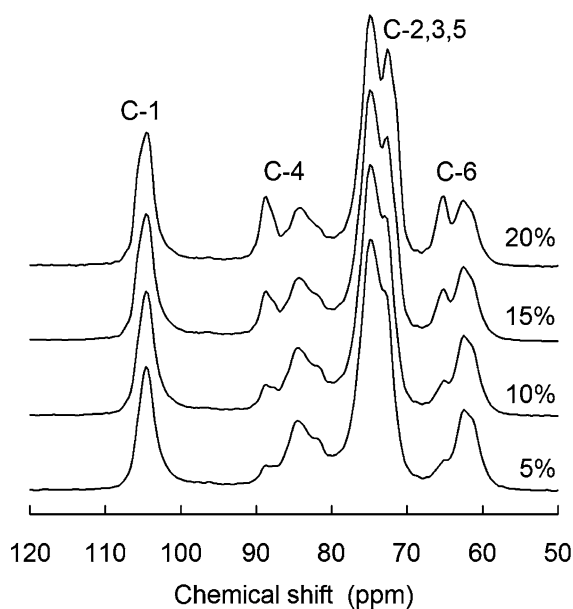
Fig. 4, interpreted according to the same procedure, indicated a crystallite width of $L = 6.3$ nm for activated MCC (Table 1).

Figure 5 shows ^{13}C NMR spectra of the composites regenerated after a dissolution time of 8 h. Peaks are assigned to cellulose I, as in Fig. 4. Cellulose II would have contributed a peak at 108 ppm, assigned to C-1 in crystallite-interior chains (Hemmingson and Newman 1995; Newman and Hemmingson 1995). No such peak was detected in Fig. 5, so there was no evidence for regeneration to cellulose II in crystallites of sufficient size for chains to be enclosed.

A peak at 89 ppm was assigned to C-4 peak of crystallite-interior chains of cellulose I. This peak was observed in all of the spectra in Fig. 5, but decreased with decreasing values of c. PSRE was used to split the NMR spectra into subspectra labeled **A** (Fig. 6), assigned to crystalline cellulose, and subspectra labeled **B** (Fig. 7), assigned to cellulose that was less well ordered.

The fraction F of cellulose associated with subspectrum A dropped steadily from 0.84 for MCC to $F = 0.24$ for the composite treated for 8 h at $c = 10\%$, then rose to $F = 0.37$ for $c = 5\%$

Fig. 4 Solid-state ^{13}C NMR spectra of activated cellulose. Experimental results are labeled **S** and **S'**. PSRE subspectra **A** and **B** are assigned to crystalline and less-ordered cellulose, respectively

Fig. 5 Solid-state ^{13}C NMR spectra of all-cellulose composites prepared from activated cellulose mixed with solvent at the weight % values shown above each trace and left for 8 h of dissolution
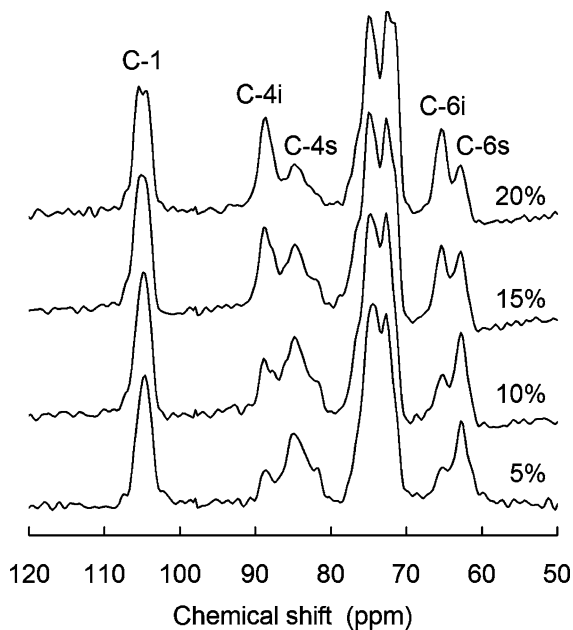
Fig. 6 Subspectra **A** separated from solid-state ^{13}C NMR spectra of all-cellulose composites prepared from activated cellulose mixed with solvent at the weight % values shown above each trace and left for 8 h of dissolution. Labels C-4i and C-4s indicate chemical shifts for chains in the interior and on surfaces, respectively, of cellulose I crystallites

Fig. 7 Subspectra **B** separated from solid-state ^{13}C NMR spectra of all-cellulose composites prepared from activated cellulose mixed with solvent at the weight % values shown above each 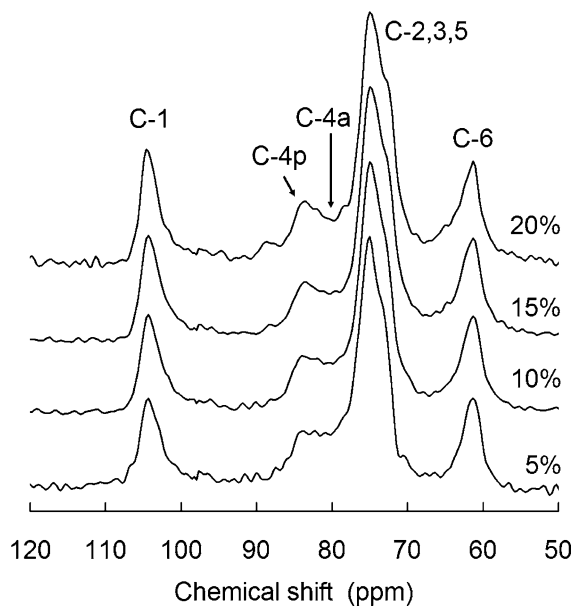trace and left for 8 h of dissolution. Labels C-4a and C-4p indicate chemical shifts for amorphous and para-crystalline cellulose, respectively

(Table 1). The last of these values might have been distorted by the difficulty in separating subspectra **A** and **B**.

Relative peak areas within subspectrum **A** were used to calculate X, i.e., the crystallite-interior cellulose expressed as % of crystalline cellulose contributing to subspectrum **A**. The values (Table 1) confirmed the visual impression (Figs. 5, 6) of a steady decline in X as the value of c was decreased. The values of X were used to calculate crystallite widths L, according to Eq. (5). Values (Table 1) indicated a decrease to $L = 2.3$ nm for the most severe treatment.

The chemical shift for C-4 is particularly sensitive to the conformation of a cellulose chain (Horii et al. 1987). Chemical shifts in the range 79 to 81 ppm are characteristic of the random-coil conformation of cellulose dissolved in trifluoroacetic acid (Bock et al. 1991) or regenerated as amorphous cellulose (Hirai et al. 1990; Newman and Hemmingson 1995). Chemical shifts in the range 84–90 ppm are characteristic of the linear conformations of chains in crystalline cellulose (Horii et al. 1987). El-Kafrawy

(1982) dissolved cellulose in LiCl/DMAc and observed a C-4 peak at 79 ppm, confirming a true solution of random-coil cellulose. All of the traces in Fig. 7 showed a dip at 80 ppm, labeled C-4a, but the fact that the dip did not extend to the baseline suggested a contribution from amorphous cellulose. Most of the C-4 signal area was found in a peak at 84 ppm, i.e., the same chemical shift as reported for C-4 in cellulose chains in linear molecular conformations exposed on the surfaces of cellulose I, with hydroxymethyl groups in the *gauche-gauche* conformation (Newman and Davidson 2004). The C-6 signal area was found in a peak at 62 ppm, also consistent with chains exposed on surfaces of cellulose I (Newman and Davidson 2004). It is possible to construct models for crystallites of cellulose I in which all chains are exposed on surfaces, but the widths must be no more than 2 nm. Such crystallites might be described as 'paracrystalline', so we have used the label C-4p in Fig. 7.

The combination of C-4 and C-6 peaks at 84 and 62 ppm, respectively, has also been reported for the NMR spectrum of cellulose IV (Isogai et al. 1989). This is consistent with a suggestion that cellulose IV

is simply a poorly crystalline form of cellulose I (Tsuda and Mukoyama 1957; Wada et al. 2004). Cellulose IV has been identified as a product of the viscose process for regenerating cellulose (Tsuda and Mukoyama 1957).

Chemical shifts for crystallite-surface chains in cellulose II have been reported as 88.0 and 86.5 ppm (C-4s) and 63.2 and 62.9 ppm (C-6s) (Newman and Davidson 2004). Those chemical shifts differ from the values observed in Fig. 7. Hong et al. (1998) reported evidence for cellulose III in cellulose fibre regenerated from LiCl/DMAc. The chemical shifts for crystallite-interior cellulose III are similar to those for cellulose II (Isogai et al. 1989), but crystallite-surface signals have not been reported.

The relevant proton spin relaxation time constants provide clues to the nature of the matrix. The experiments described in this paper were based on differences in $T_2(H)$ between crystallites and the matrix. Subspectra were separated from spectra of the primary walls of *Arabidopsis thaliana* by Newman et al. (1996), and the values of k and k' in Eq. (3) indicated $T_2(H) = 8.5$ µs and 19 µs for crystalline cellulose and amorphous matrix polysaccharides, respectively. Using the same expressions for k and k' in the present work indicated $T_2(H) = 8.6$ µs and 11 µs for crystallites and matrix, respectively. The value of $T_2(H)$ for the cellulosic matrix was not greatly increased over the value for the crystallites, suggesting paracrystallinity rather than amorphicity.

The subspectra stacked in Fig. 7 could not be used to determine the relative proportions of paracrystalline and amorphous cellulose, since the C-4 peaks were not resolved. Overlap between the C-4 and C-2,3,5 bands might even account for much of the signal strength in the dip at 80 ppm.

Kondo et al. (2001) introduced the concept of 'nematic ordered cellulose' to cover intermediate states of molecular ordering such as those described in this work, i.e., states that display some of the features of each of the crystalline allomorphs of cellulose, yet no perfect match to any one of those allomorphs.

Comparisons between WAXS and NMR

The WAXS index CrI showed strong correlations with both of the NMR indices tabulated in Table 1. Linear least-squares fits gave correlation coefficients

$R^2 = 0.92$ and 0.94 for CrI against F and X respectively. The correlation coefficient rose to $R^2 = 0.99$ for CrI against the product FX, i.e., crystallite-interior cellulose expressed as % of total cellulose.

The crystallite dimensions D and L showed similar trends, i.e., decreasing cross-sectional dimensions as a result of partial dissolution. A perfect match was not expected for these parameters, since they represent cross-sectional measurements in orthogonal directions: D perpendicular to the (200) planes, L across those planes (Newman 1999).

Transformation mechanisms

When considered together, the WAXS and NMR results suggest the following mechanism.

Exposure to LiCl/DMAc peels layers of cellulose from crystallites. The residual core of the crystallite becomes thinner as successive layers are removed. The peeled layers might retain some of the molecular ordering of the cellulose I structure from which they were removed, but are too thin to contain crystallite-interior chains. When the LiCl and DMAc are washed away, the peeled layers of cellulose are regenerated into a paracrystalline matrix. The paracrystalline structures are sufficiently disordered to show $T_2(H)$ values slightly longer than those characteristic of crystalline cellulose. On the other hand, they are sufficiently distinct from amorphous cellulose to show a WAXS peak just half as broad. They are also sufficiently distinct to show a 4 ppm displacement of the C-4 ^{13}C NMR peak, from 80 ppm for amorphous cellulose to 84 ppm for the matrix of the composites.

The partly ordered nature of the matrix helps account for the superior mechanical properties observed for all-cellulose composites.

Using relatively high concentrations of cellulose in LiCl/DMAc has several advantages. Above all else, it minimizes the shrinkage undergone by the material during the precipitation and drying stage. This minimizes many manufacturing constraints like large mould opening, shape loss or amount of residual water in the material before drying. There are also financial, environmental and health interests in minimizing the amount of solvent used for a given amount of polymer. Conio et al. (1984) suggested that a concentration $c < 15\%$ was necessary for partial

dissolution in 8% LiCl/DMAc, and a concentration c < 11% was necessary for complete dissolution. Our results show that partial dissolution could be observed at c = 20%. More work is required to test whether the degree of transformation was sufficient to provide satisfactory mechanical properties. Transformation was nearly complete for c = 10%, but we detected a trace of residual crystalline cellulose.

Conclusions

Partial dissolution and regeneration of cellulose, using LiCl/DMAc, yields all-cellulose composites with a matrix comprising a mixture of paracrystalline and amorphous cellulose. Both WAXS and NMR results point to distinct differences from a fully amorphous matrix. More work is needed to test the consequences of paracrystallinity on the mechanical properties of all-cellulose composites.

References

Bledzki AK, Gassan J (1999) Composites reinforced with cellulose based fibres. Progr Polymer Sci 24:221–274

Bock B, Bock S, Fengel D (1991) NMR parameters of cellulose in TFA solution. Holzforschung 45:321–324

Conio G, Corazza P, Bianci E, Taldi A, Ciferri A (1984) Phase-equilibria of cellulose in N,N-dimethylacetamide/LiCl solutions. J Polymer Sci Part C - Polymer Lett 22:273–277

Dupont A-L (2003) Cellulose in lithium chloride/N,N-dimethylacetamide, optimisation of a dissolution method using paper substrates and stability of the solutions. Polymer 44:4117–4126

El-Kafrawy A (1982) Investigation of the cellulose/LiCl/dimethylacetamide and cellulose/LiCl/N-methyl-2-pyrrolidone solutions by ^{13}C NMR spectroscopy. J Appl Polymer Sci 27:2435–2443

Gindl W, Keckes J (2004) Tensile properties of cellulose acetate butyrate composites reinforced with bacterial cellulose. Composites Cellulose Technol 64:2407–2413

Gindl W, Keckes J (2005) All-cellulose nanocomposite. Polymer 46:10221–10225

Gindl W, Martinschitz KJ, Boesecke P, Keckes J (2006a) Structural changes during tensile testing of an all-cellulose composite by in situ synchrotron X-ray diffraction. Composites Sci Technol 66:2639–2647

Gindl W, Schöberl T, Keckes J (2006b) Structure and properties of a pulp fibre-reinforced composite with regenerated cellulose matrix. Appl Phys A – Mater Sci Processing 83:19–22

Gjønnes J, Norman N (1958) The use of half width and position of the lines in the X-ray diffractograms of native cellulose to characterize the structural properties of the samples. Acta Chemica Scandinavica 12:2028–2033

Gjønnes J, Norman N (1960) X-ray investigations on cellulose II and mixtures of cellulose I and II. 2. Lateral order in cellulose II. Acta Chemica Scandinavica 14:689–691

Glasser WG, Taib R, Jain RK, Kander R (1999) Fiber-reinforced cellulosic thermoplastic composites. J Appl Polymer Sci 73:1329–1340

Hemmingson JA, Newman RH (1995) Changes in molecular ordering associated with alkali treatment and vacuum drying of cellulose. Cellulose 2:71–82

Hirai A, Horii F, Kitamaru R (1990) Carbon-13 spin-lattice relaxation behaviour of the crystalline and noncrystalline components of native and regenerated celluloses. Cellulose Chem Technol 24:703–711

Hong Y-K, Chung K-H, Lee W-S (1998) Structure of regenerated cellulose fibers from DMAc/LiCl solution. Textile Res J 68:65–69

Horii F, Hirai A, Kitamaru R (1987) Cross-polarization-magic angle spinning carbon-13 NMR approach to the structural analysis of cellulose. In: Atalla RH (ed) The structures of cellulose: characterization of the solid states. American Chemical Society, Washington DC, p 119

Ioelovich M, Larina E (1999) Parameters of crystalline structure and their influence on the reactivity of cellulose I. Cellulose Chem Technol 33:3–12

Ishii D, Tatsumi D, Matsumoto T (2003) Effect of solvent exchange on the solid structure and dissolution behavior of cellulose. Biomacromolecules 4:1238–1243

Isogai A, Usuda M, Kato T, Uryu T, Atalla RH (1989) Solid-state CP/MAS ^{13}C NMR study of cellulose polymorphs. Macromolecules 22:3168–3172

Kondo T, Togawa E, Brown Jr RM (2001) ''Nematic ordered cellulose'': a concept of glucan chain association. Biomacromolecules 2:1324–1330

Kroon-Batenburg LMJ, Kroon J, Northolt MG (1990) Theoretical studies on β(1→4) glucose oligomers as models for native and regenerated cellulose fibres. Das Papier 44:640–647

Lu JZ, Wu QL (2000) Chemical coupling in wood fiber and polymer composites: A review of coupling agents and treatments. Wood Fiber Sci 32:88–104

Mann J (1962) Modern methods of determining crystallinity in cellulose. Pure Appl Chem 5:91–105

McCormick CL, Callais PA, Brewer Jr HH (1985) Solution studies of cellulose in lithium chloride and N,N-dimethylacetamide. Macromolecules 18:2394–2401

Murdock CC (1930) The form of the X-ray diffraction bands for regular crystals of colloidal size. Phys Rev 35:8–23

Newman RH (1999) Estimation of the lateral dimensions of cellulose crystallites using 13C NMR signal strengths. Solid State Nuclear Magnetic Resonance 15:21–29

Newman RH, Davies LM, Harris PJ (1996) Solid-state ^{13}C nuclear magnetic resonance characterization of cellulose in the cell walls of *Arabidopsis thaliana* leaves. Plant Physiol 111:475–485

Newman RH, Davidson TC (2004) Molecular conformations at the cellulose-water interface. Cellulose 11:23–32

Newman RH, Hemmingson JA (1995) Carbon-13 NMR distinction between categories of molecular order and disorder in cellulose. Cellulose 2:95–110

Nishino T, Matsuda I, Hirao K (2004) All-cellulose composite. Macromolecules 37:7683–7687

Nishino T, Takano K, Nakamae K (1995) Elastic modulus of the crystalline regions of cellulose polymorphs. J Polymer Sci: Part B: Polymer Phys 33:1647–1651

Schroeder LR, Gentile VM, Atalla RH (1986) Nondegradative preparation of amorphous cellulose. J Wood Chem Technol 6:1–14

Segal L, Creely JJ, Martin AE, Conrad CM (1959) An empirical method for estimating the degree of crystallinity of native cellulose using the X-ray diffractometer. Textile Res J 29:786–794

Striegel AM (2002) Advances in the understanding of the dissolution mechanism of cellulose in DMAc/LiCl. J Chilean Chem Soc 48:73–77

Sugiyama J, Vuong R, Chanzy H (1991) Electron diffraction study on the two crystalline phases occurring in native cellulose from an algal cell wall. Macromolecules 24:4168–4175

Tsuda Y, Mukoyama S (1957) The formation of cellulose IV in the viscose spinning. Bull Chem Soc Jpn 30:718–720

Wada M, Heux L, Sugiyama J (2004) Polymorphism of cellulose I family: reinvestigation of cellulose IV. Biomacromolecules 5:1385–1391

Yano H, Sugiyama J, Nakagaito AN, Nogi M, Matsuura T, Hikita M, Handa K (2005) Optically transparent composites reinforced with networks of bacterial nanofibers. Advanced Materials 17:153–155

Yamashiki T, Matsui T, Kowsaka K, Saitoh M, Okajima K, Kamide K (1992) New class of cellulose fiber spun from the novel solution of cellulose by wet spinning method. J Appl Polym Sci 44:691–698